ELSEVIER
SAUNDERS

Thorac Surg Clin 14 (2004) 135–149

THORACIC
SURGERY
CLINICS

Future generation CT imaging

Deborah Walter, PhD*, Bruno De Man, PhD, Maria Iatrou, PhD,
Peter M. Edic, PhD

Computed Tomography Systems and Applications Laboratory, GE Global Research Center, One Research Circle, Niskayuna, NY 12309, USA

Since the 1970s CT has been used to generate cross-sectional images of human anatomy from x-ray projection data acquired at many angular positions around the body. The development of the first CT scanner is credited to Hounsfield [1], using reconstruction methods developed by Cormack [2]. Since then several key technological advancements have increased the usefulness of CT to the point where it has become an essential tool in the clinical evaluation of patients, with most hospitals having CT scanners available 24 hours a day, 7 days a week. First-generation CT systems, which used a single, thin x-ray beam and a single detector element to acquire the x-ray projection data necessary for image reconstruction, quickly evolved into third-generation systems, which use a fan-shaped x-ray beam combined with a rotating x-ray tube and detector to acquire the x-ray projection data needed for image reconstruction. With the development of helical CT systems in the late 1980s [3–6], large sections of anatomy could be scanned quickly using linear, continuous table motion, enabling faster throughput and better registration between adjacent slices of the body. Electron beam CT (EBCT) technology, incorporating a stationary detector and using an x-ray tube comprised of a stationary target ring and a swept electron beam, was developed in 1983 to scan the heart and coronary arteries at subsecond scan times, thereby reducing motion artifacts resulting from the beating of the heart during data acquisition [7]. Recently, CT has further evolved from single-slice scanners to systems incorporating multiple detector rows with improved resolution, with the introduction of multislice CT (MSCT) in 1998, enabling high-resolution, thin-slice scanning of large sections of human anatomy.

Over the years CT scanning has found widespread use in imaging applications for trauma assessment, thoracic and vascular studies, and stroke assessment, as well as emerging applications in cardiac imaging, lung cancer detection, colonoscopy, and brain and myocardial perfusion. The goal of this article is to outline some of the recent technological advances that will drive future CT evolution and to describe the recently enabled applications and trends in chest imaging.

Image acquisition aspects

Image acquisition with today's multislice scanner is more flexible when compared with a single-slice scanner because many scanning modes are made available to the clinician. For example, several combinations of slice thickness and helical pitch can now be used to scan the full thorax within a single breath-hold, giving clinicians many options to maximize the clinical value of the acquired images. Because more protocol options are available to the clinician, it is important to understand the relationship between scanner parameters and resulting image quality so that the acquisition can be tailored to meet the particular imaging need. Some of the key geometric parameters are identified in Fig. 1, a third-generation CT system.

Two important characteristics to consider when thinking about CT image quality are spatial resolution and image noise. The key imaging parameters

* Corresponding author.
E-mail address: walter@research.ge.com (D. Walter).

1547-4127/04/$ – see front matter
doi:10.1016/S1547-4127(04)00040-4

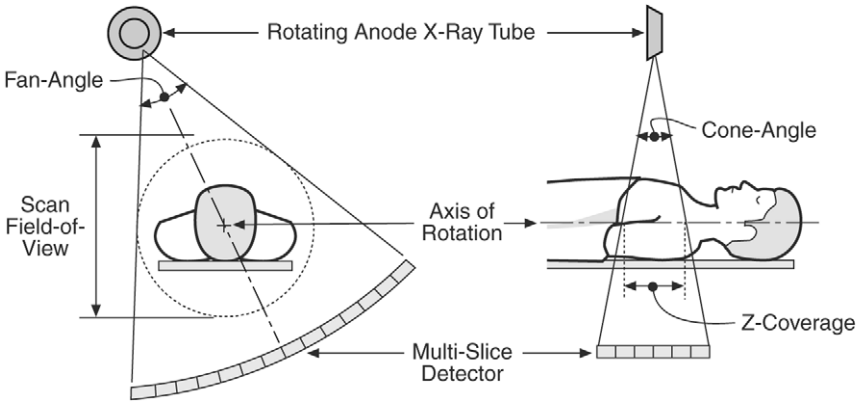

Fig. 1. Third-generation multislice CT scanner. Front view (*left*) shows the x-ray tube and the x-ray detector. The patient lies along the axis of rotation. The scan field of view is the circular region inscribed in the rotating fan beam. The side view (*right*) shows the relationship between the cone angle, the longitudinal size of the detector, and the z-coverage, which is measured at the isocenter. The z-dimensions are strongly exaggerated for clarity.

that affect spatial resolution in reconstructed images are the

- Size of the focal spot in the x-ray tube
- Length, width, and configuration of the detector cells
- Location and number of angular positions at which x-ray projection data are acquired as the x-ray source and detector rotate around the patient
- Filter used to preprocess the x-ray projection data before image reconstruction
- Helical pitch ratio prescribing the table speed

The key imaging parameters that affect image noise are the size and anatomy of the patient being scanned, the operating voltage and current of the x-ray tube, the rotational speed of the gantry comprising the x-ray tube and detector, in addition to all of the parameters that affect spatial resolution.

The main source of image noise in reconstructed CT images is the statistical nature of x-ray photons. For each detector channel the deviation of the measured attenuation of x-rays along a particular direction from the true attenuation value decreases as the number of detected photons increases. Consequently, image noise decreases with increased x-ray tube current (at the expense of increased patient dose), increased detector size (at the expense of decreased spatial resolution), and reduced attenuation (in a small patient or low-density objects such as lungs). Given the complex relationships between the imaging parameters and their impact on image quality, future imaging protocols will likely migrate from specifying individual acquisition parameters to specifying image quality and dose requirements, enabling the optimal acquisition protocol to be implemented on the scanner [8,9].

Technological advances and trends

Since its conception in the early 1970s CT has undergone an enormous metamorphosis. The first CT scanners [1] produced a 1 cm thick slice in about 4 minutes. Current scanners can produce 16 slices at submillimeter resolution in less than 1 second [10–13]. The following sections describe what the authors believe are currently the major trends in CT scanner technology development.

Spatial resolution

Today, modern medical CT scanners can resolve objects that are less than 1 mm in size. Nevertheless, many applications would benefit from the ability to visualize even smaller structures. In particular, clinicians are interested in isotropic spatial resolution (ie, the longitudinal resolution is equally good as the in-plane resolution). Isotropic resolution allows the clinician to visualize reconstructed data along various planar reformats without loss of detail in the images.

The spatial resolution of a CT scanner is limited by several factors: the effective size of the x-ray tube focal spot, the size of the individual detector cells, the data sampling pattern implemented by the imaging geometry, and the stages in the reconstruction algorithm. It is important to realize that spatial resolution

is not equal to the image pixel/voxel size but is an intrinsic property of the scanner. Therefore, the operator must adjust the pixel size by appropriately selecting the field of view of the reconstruction so that it is not a limiting factor of spatial resolution. To develop CT scanners that have increased spatial resolution, one has to reduce the focal spot size, reduce the detector cell size, and increase the number of angular positions at which x-ray projection data are acquired. The increased number of detector channels, the increased number of views, and the increased number of reconstructed image voxels result in much larger datasets, meaning larger computation times and larger storage requirements. To maintain an acceptable noise level at higher spatial resolution, one has to increase the x-ray flux, resulting in an increased patient dose (see section on dose reduction in this article). Using a smaller focal spot size limits the maximum output flux from the x-ray tube for thermal reasons, resulting in higher image noise.

Researchers at the GE Global Research Center developed a number of research CT scanners recently based on a flat panel detector consisting of a grid of 1024 × 1024 detector cells, each 200 μm × 200 μm in size, to explore the clinical impact of higher spatial resolution in combination with large volume coverage [14]. Fig. 2A shows the image of a plastinated dog lung phantom scanned on a Lightspeed clinical scanner (GE Medical Systems, Milwaukee, Wisconsin). Fig. 2B shows GE's volumetric CT research system. The improvement in the image sharpness demonstrates the resolution improvement that is possible in future CT scanners.

Volume coverage

From CT's conception until the late 1990s, CT data have always been acquired one slice at a time. One exception was CT Twin (Elscint, Haifa, Israel), a dual-slice CT scanner made in 1992. It was not until 1998 that four manufacturers (GE, Siemens, Toshiba, and Marconi) manufactured a four-slice CT scanner simultaneously. The most recent commercial scanners allow the acquisition of 16 slices simultaneously [10–13]. The basic principle behind multislice CT involves stacking a number of detector rows longitudinally (Fig. 3) [15,16], which explains why some people use the term multidetector instead of multislice, although strictly speaking it is still one detector consisting of a two-dimensional array of detector cells. Typically, the detector consists of a larger number of detector rows that are binned together longitudinally depending on the desired slice thickness. Some manufacturers prefer to use thinner detector rows in the center and thicker detector rows at the ends; other manufacturers prefer to use detector rows of equal size.

The main advantage of multislice scanners is the ability to scan a given volume in a shorter time, or vice versa, scan a larger volume within a given time. This ability has an enormous impact on clinical applications, as discussed in more detail in the

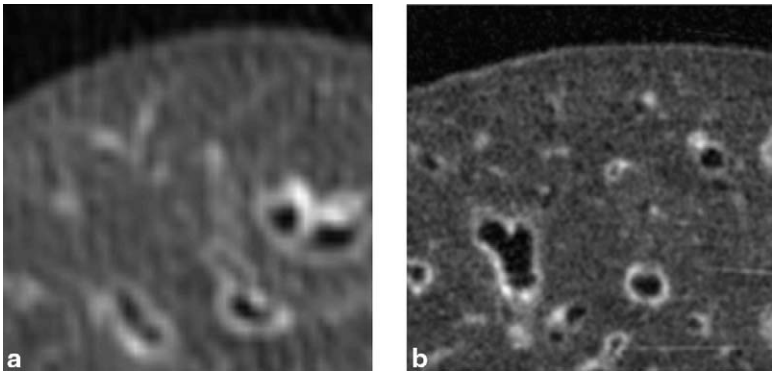

Fig. 2. High-resolution axial image of plastinated dog lung phantom. Both images represent a region of interest of approximately 1.8 cm^2. (*a*) This image was obtained with a GE Lightspeed system at 120 kVp, 100 mA, 4 × 1.25 mm detector collimation, a helical pitch of 1.5:1, and reconstructed with the bone kernel. (*b*) The image is the same phantom imaged on a GE high-resolution volumetric CT prototype system capable of 250 μm isotropic resolution. The two images are not registered; however, by comparing features of similar size, the high-resolution volumetric CT image demonstrates the resolving power that could be achieved in future commercial CT scanners. Because the lung tissue was dried before plastination, all vessels appear to be filled with air. (CT image courtesy of Rebecca Fahrig, PhD Stanford University, Stanford, CA; high-resolution volumetric image courtesy of GE Global Research Center, Niskayuna, NY; phantom developed by Dr. Robert Henry, University of Tennessee.)

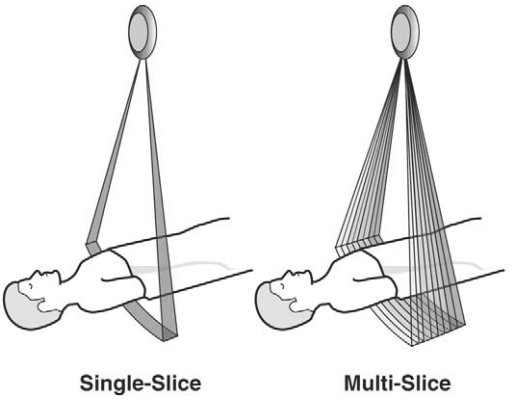

Fig. 3. Comparison of single-slice and multislice CT scanner. A single-slice CT scanner has only one detector row. In multislice CT, the detector consists of multiple rows that are stacked longitudinally and can be configured in one of several topologies for various choices of slice thickness. The x-ray source illuminates multiple rows simultaneously. A 16-slice scanner can read out 16 slices simultaneously.

clinical imaging applications section of this article. Detectors that have wider coverage could eventually allow organ imaging in a fraction of the time required today. This advantage could remove the demand for faster gantry rotational speeds, and it would enable the imaging of a whole organ for perfusion studies in a single rotation.

One issue that needs to be taken into account when using larger scan coverage per rotation is the increased cone angle (see Fig. 1), the longitudinal angle at which the source covers the detector. The cone angle has two implications. First, the relative amount of scattered radiation increases almost linearly with the size of the cone angle. Second, and perhaps more important, as the cone angle increases, it becomes more difficult to reconstruct high-quality images based on the measured data. For smaller cone angles such as those of 16-slice scanners, the algorithms for single-slice CT are still sufficiently accurate, at least with some minor modifications. The most famous adaptation is the so-called Feldkamp reconstruction approach [17], in which the classic fan beam algorithm is adapted to take into account the true geometry of the cone beam acquisition; however, these adaptations are still approximations, and for larger cone angles they become too inaccurate, resulting in cone beam image artifacts. For larger cone angles with axial (nonhelical) CT scans it becomes mathematically impossible to perform an exact reconstruction because of incomplete data.

Two solutions have been proposed to handle this problem. The first solution is to acquire complete data using circle-plus-line or circle-plus-arc trajectories, in which a small linear scan accompanies each rotation, similar to a scout scan in conventional CT [18]. The second solution is to take large cone angle helical CT acquisitions, in which exact reconstruction remains theoretically possible. Tuy [19] and Grangeat [20] showed how cone beam measurements could be used for mathematically exact image reconstruction. Based on this work several exact, wide cone beam algorithms have been published recently [21–23]. For ease of implementation, a number of approximate algorithms have been proposed [24,25]. With the prospect of CT geometries with larger and larger cone angles, research in cone beam reconstruction has become an active field in the past few years.

Temporal resolution

Another trend in CT is the ever-increasing acquisition speed, which is important for two reasons: (1) to avoid motion artifacts caused by, for instance, cardiac motion, breathing, or patient movement, and (2) to reduce the total scan time for one examination. Reducing the scan time prevents slice misregistration, facilitates studies with contrast agents, and decreases patient examination time.

The straightforward way to improve temporal resolution is to increase the gantry rotation speed; however, rotating a 1 ton gantry at two rotations per second or more results in extremely challenging mechanical constraints. Another problem is that large amounts of data have to be transmitted in a shorter time. Finally, and most important to the clinician, faster scanning limits the total number of x-ray photons that the x-ray tube can deliver per scanned slice, resulting in images that have increased noise. One way to overcome the speed limitation is to use a large, stationary circular detector, replace the x-ray tube with an electron gun, producing a beam of electrons directed on a large stationary circular target, and sweep this electron beam around the target to scan the patient. This technique is the basis of the EBCT scanner [7,26]. The absence of moving parts allows scan speeds equivalent to a "rotation" time of about 50 ms, or 10 × faster than conventional CT scanners.

The most challenging application for CT and other noninvasive imaging modalities is cardiac imaging because of the dynamic nature of the heart. For cardiac imaging, particularly CT angiography, there is a demand for improved image quality (ie, better spatial and temporal resolution, whole-heart scanning in one breath-hold, improved signal-to-noise ratio, and low-contrast detectability for determining functional information). These characteristics drive the technology

toward faster rotational speeds for the gantry, wider coverage, more efficient detectors, and advanced reconstruction techniques. The volume of the heart changes drastically during the cardiac cycle. Therefore, if the imaging system could acquire the necessary projection data for reconstruction of the heart during a phase of minimum motion, the resulting image quality would contain reduced motion artifacts. High temporal resolution is required to freeze the heart motion, and high spatial resolution is needed to allow clinicians to identify and characterize coronary arteries, enabling visualization and quantification of stenotic segments and discernment of constituent components of atherosclerotic plaque that might be present [27–30]. Fig. 4 shows an image of restenosis in a stent of the proximal left anterior descending coronary artery from data acquired with a multislice CT system at 0.625 mm slice thickness (Lightspeed 16, GE Medical Systems, Milwaukee, Wisconsin) and reconstructed with a multisector approach. Sectors of x-ray projection from multiple rotations of the gantry are combined to provide the data necessary for image reconstruction at 0.3 mm intervals with overlapping slices [28,29,31].

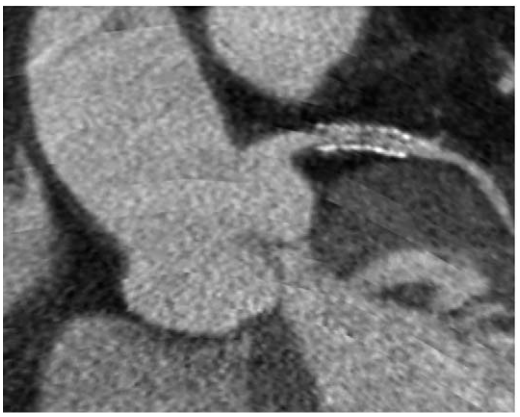

Fig. 4. Cardiac imaging using a multisector reconstruction approach. The image shows restenosis in a stent placed in the proximal left anterior descending coronary artery. Data were acquired with a clinical CT scanner configured with 0.625 mm slice thickness (GE Lightspeed 16) and reconstructed with a multisector approach at 0.3 mm intervals with overlapping slices. Using state-of-the-art CT imaging technology and multisector reconstruction algorithms, today's scanners have capabilities that approach the spatial resolution and the temporal resolution needed to evaluate the coronary arteries of the heart. The heart rate of this patient during this examination ranged between 71 beats per minute and 82 beats per minute. (Courtesy of J.L. Sablarolles, MD, Centre Cardiologique Du Nord, Saint Denis, France.)

Dose reduction

No aspect of medical CT imaging has received more attention in recent years than patient radiation dose [32–34]. For diagnostic imaging in general, the radiation dose should be kept to as low as reasonably achievable while maintaining suitable diagnostic capability for features of interest. Radiation dose measurements are reported in the CT–dose index (CTDI, in Gy), dose–length–product (in mGy-cm), and effective dose (in mSv). CTDI standards are useful to objectively rate different scan protocols available in a scanner and among different types of scanners, but the dose index is not useful in predicting the image quality (ie, noise level) produced in anatomical imaging or the risk to the patient. The computation of effective dose is used to rate the relative risk to patients from radiologic procedures [35,36]. For the calculation of this quantity, the absorbed dose is calculated in specific organs or tissues and is weighted by the relative sensitivity of these tissues to x-ray radiation to predict risk to the patient (ie, tissue weighting factors).

The noise and the quality of the diagnostic information available in an image depend on the interplay between the data acquisition parameters (eg, helical pitch, detector collimation, tube current, tube voltage, x-ray beam filtering), the reconstruction approach (eg, helical weighting, reconstruction kernel, longitudinal smoothing), and the postprocessing techniques (eg, thresholding, segmentation, volumetric measurements). Image noise also depends on the patient's anatomy. In modern CT scanners, the detector's efficiency (its ability to absorb an x-ray of a certain energy) is near its theoretical limit; therefore, other options must be explored to reduce patient doses.

Several techniques have been suggested to optimize the information available in CT imaging or to reduce the dose delivered to the patient. Two general approaches are to: (1) reduce the dose by modulating the intensity of the x-rays, and (2) use the measurements in an optimal scheme to improve the diagnostic information for a given dose.

One of the latest features on some multislice scanners is the ability to modulate the tube current for different sections of the body. The x-ray tube current is increased along lateral directions in the patient, where there is significant attenuation (eg, along the shoulders), and reduced along anterior–posterior directions, where less attenuation is encountered as the x-ray tube and detector rotate around the body. The x-ray tube current is also varied in a global sense as the patient is translated horizontally with the patient table in the helical scanning mode as the

natural contour of the human body increases or decreases. In both cases the x-ray tube current is adjusted appropriately to meet a noise requirement that is set by the radiologist (see [37] and references therein). These techniques have been shown to reduce the dose delivered to the patient significantly, but it is critical to set an appropriate noise factor that does not inhibit diagnostic information. In the future all CT scanners will use such techniques.

One way to optimize dose usage is to make the measured intensities more uniform within each x-ray projection (denoted as a view), which is accomplished by using specially shaped filters (eg, bowtie filters). Central rays usually traverse larger sections of the patient and are therefore filtered minimally by the bowtie filter. Peripheral rays in the x-ray beam usually traverse smaller sections of the patient and are therefore filtered more. The net result is that all rays undergo roughly the same amount of attenuation. This technique reduces the harmful absorbed dose at the peripheral of the body [38]. As the radiological community continues to advocate lower doses, one can conceive of special x-ray beam filtering techniques that could be optimized for a specific organ of interest.

Current multislice helical reconstruction algorithms based on the filtered backprojection method use a variety of weighting and filtering schemes to trade off noise and artifacts in the reconstructed image with the achievable spatial resolution. A particularly difficult area in the body for low-dose imaging is the region near the shoulders. These slices usually suffer from structured noise, which appears as horizontal streaks across the image, because of the significant attenuation of the x-ray signal through the shoulders. Various schemes have been proposed to improve the signal-to-noise ratio of measurements acquired along projection lines with significant attenuation by using information from neighboring detector cells or views. In some cases special filtering schemes also incorporate signals measured in the longitudinal direction from data measured with the multislice detector [24,39,40]. To demonstrate one such scheme, Fig. 5 displays a scan of the right lung of a human patient. On the left (Fig. 5a) the chest was scanned using an x-ray beam current of 200 mA. In the middle (Fig. 5b) the same anatomy is scanned with much lower dose, using an x-ray current of 10 mA. On the right (Fig. 5c) the data used to generate the image shown in Fig. 5b are reconstructed using an adaptive filtering scheme incorporated as part of the reconstruction algorithm [39]. Although the adaptive filtering algorithm reduces spatial resolution slightly, as demonstrated in Fig. 5c, the benefits of reduced image noise are shown clearly.

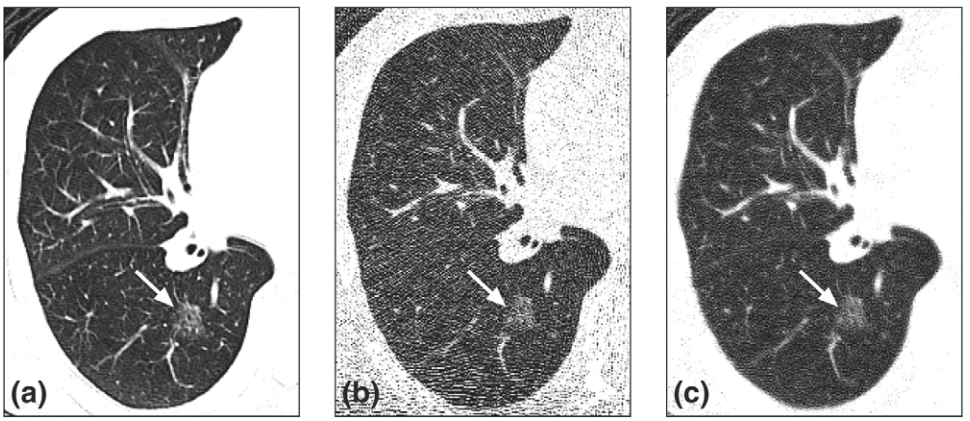

Fig. 5. Adaptive filtering to reduce noise artifacts for low-dose imaging. The scan of the right lung of this patient shows a nonsolid pulmonary nodule (*arrow*). (*a*) Image reconstructed from x-ray projection data acquired using a system configuration of 120 kVp, 200 mAs, 0.5 s gantry speed (100 mAs), 4 × 2.5 mm detector collimation, and a helical pitch ratio of 0.75:1 using a GE Lightspeed Plus (GE Medical Systems, Milwaukee, Wisconsin). (*b*) The same anatomy was scanned at much lower dose; the image was reconstructed from x-ray projection data acquired using a system configuration of 120 kVp, 10 mA, 0.5 s gantry speed (5 mAs), 4 × 1.5 mm detector collimation, and a helical pitch ratio of 1.5:1. (*c*) The same x-ray projection data used to generate the image shown in (*b*) was reconstructed using a reconstruction algorithm incorporating adaptive filtering techniques. In all three images the nodule is visible; however, the image shown in (*c*), which was reconstructed using adaptive filtering techniques, contains less noise artifact when compared with the image in (*b*), at a slight reduction in the spatial resolution when compared with the image in (*a*). (Courtesy of Akifumi Fujita, MD, Showa University, Fujigaoka Hospital.)

Another strategy to reduce noise in CT images or to achieve the same noise level at reduced dose is the use of statistical reconstruction algorithms, which weigh x-ray projection data in an optimal sense for CT image reconstruction. Although statistical reconstruction algorithms have been investigated in nuclear medicine for many years, they have not yet been commonly used for CT image reconstruction mainly because of the computational complexity of such approaches and the fact that the signal-to-noise ratio in x-ray projection measurements is higher in CT compared with nuclear imaging. Unlike filtered backprojection reconstruction approaches, statistical reconstruction has a framework that includes a statistical model for the measurements. More recently, several researchers have applied statistical reconstruction to CT successfully [41–44]. Statistical reconstruction also allows incorporation of prior information regarding the scanned region of interest (ROI) to improve image quality in reconstructed images in an efficient manner. Apart from minimizing image noise, statistical reconstruction has also been shown to have potential for artifact reduction [42,43] and for applications with missing x-ray projection data needed for image reconstruction [45–47].

Clinical imaging applications

New scanners that have improved algorithms and technology offer superior image resolution, greater coverage, and shorter acquisition times. As a result of advancing CT imaging technology, the amount of information required for physicians to review has also increased. To improve clinicians' workflow and productivity, three-dimensional image processing algorithms, advanced workstations, and computer-assisted tools have been developed. Advanced postprocessing tools have many applications and have been shown to improve accuracy and productivity [48,49]. Some specific examples of advanced CT technology combined with computer-assisted tools are discussed in this section.

Lung cancer

The American Cancer Society has estimated that 171,900 new lung cancer cases would be diagnosed and 157,200 lung cancer deaths would occur in the United States in 2003 [50]. CT imaging currently plays an important role in all aspects of lung cancer management including detection, diagnosis, staging, treatment planning, and patient follow-up care [51–61]. In the past decade, spatial resolution achievable with state-of-the-art CT scanners has increased more than tenfold. CT now routinely provides detailed images of early-stage lung cancer by imaging with a spatial resolution of less than 1 mm. High-resolution imaging has led to significant advances in clinical understanding of early disease progression and has redefined lung cancer management practices. This section focuses on state-of-the-art and emerging CT applications in the area of lung cancer and describes the impact of future technological improvements.

Solitary pulmonary nodule detection and sizing

The superiority of CT over other radiologic imaging techniques (eg, chest radiograph, MRI) for the detection of solitary pulmonary nodules (SPNs) is well documented [62–64]. Recent technological advancements in multislice CT, namely the ability to scan the entire human thorax at submillimeter resolution within a breath-hold, enable the detection of much smaller lesions [63,65]. This realization has spurred several studies to reinvestigate the hypothesis that the early detection of lung cancer could justify screening for lung cancer in asymptomatic patients (see [51] for a review of current lung cancer screening literature).

In addition to enabling the detection of small SPNs, high-resolution CT imaging has also been shown to be a highly sensitive for the measurement of small changes in volume [61,66,67]. Radiologic phantom studies, used to characterize the sensitivity of high-resolution CT imaging for growth estimation, indicate that volume accuracy using CT is within 3% of the true volume in nodules between 3 and 6 mm in diameter and within 1% in nodules greater than 6 mm in diameter [61]. These results were obtained under ideal imaging conditions: small field-of-view imaging, application of resolution-enhancing reconstruction kernels, thin-slice imaging mode, low helical pitch, and the absence of confounding anatomical structure. These results should therefore be considered an upper limit of current CT capability. The clinical evidence for in situ volumetric accuracy of nodule sizing is not conclusive for several reasons: (1) nodule sizing methods have not been standardized, (2) the highest available resolution capabilities of the scanner are not routinely used for examinations, and (3) advanced segmentation and computation tools have only become recently available.

In general, three-dimensional computer-assisted segmentation tools generate the most accurate and repeatable nodule size measurements [53]. An example case showing results from the use of advanced analysis tools is presented in Figs. 6 and 7. Fig. 6a shows a CT image of an SPN attached to a vascu-

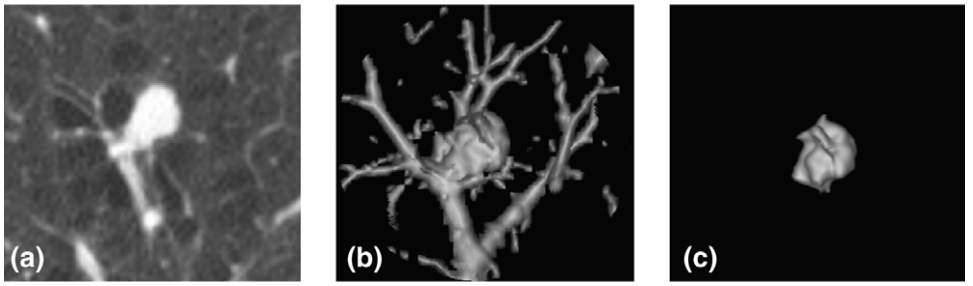

Fig. 6. Segmentation of pulmonary nodules with minimal user interaction. An SPN is detected by the radiologist, and using advanced analysis tools (Advanced Lung Analysis, GE Medical Systems, Milwaukee, Wisconsin) the nodule is segmented automatically and the volume is determined. (*a*) Solid pulmonary nodule detected by the radiologist in an axial CT scan. (*b*) The Nodule and vessel structure are segmented from the parenchyma and displayed as a three-dimensional surface. (*c*) Nodule is separated automatically from the vascular structures and its volume is computed. (Courtesy of Lawrence Goodman, MD, Froedtert Hospital, Milwaukee, WI.)

lar structure. Fig. 6b shows the nodule and vessel structure, which have been segmented from the lung parenchyma and displayed as a three-dimensional surface. The nodule was separated automatically from the vascular structure and the volume was computed. The three-dimensional surface model of the nodule separated from the vascular structure is shown in Fig. 6c.

The images in Fig. 7 show a nodule that was measured in two CT scans one month apart; the nodule size exhibits a 24% volume increase, corresponding to a 103-day doubling time, assuming exponential growth.

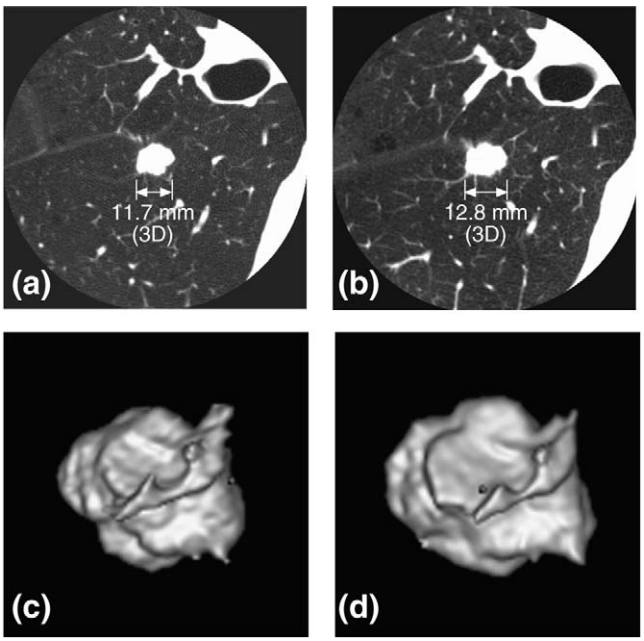

Fig. 7. Determining nodule growth rate with volumetric measurements. Multiple images of a nodule, measured 1 mo apart, are shown. The volume at each time instance was measured using GE Medical System's Advanced Lung Analysis program. (*a*) Using the CT image of the nodule measured at time one, the diameter of the nodule is shown to be 11.7 mm. (*b*) The same nodule measured one month later is 12.8 mm in diameter. (*c*) Three-dimensional surface model of the nodule measured at time one. (*d*) Three-dimensional surface model of the same nodule measured at time two. This nodule exhibited a 24% increase in volume, corresponding to a 103-day doubling time assuming exponential growth. (Courtesy of The Early Lung Cancer Action Program, New York Presbyterian Hospital, Weill Cornell Medical Center, New York, NY.)

Another revelation in the understanding of the characteristics of SPNs relates to the increased frequency of detection of subsolid lesions (or ground-glass opacities) [55,68,69]. The importance of subsolid lesions has recently become apparent because nonsolid and part-solid lesions appear to be highly correlated to malignancy. In one study, nonsolid nodules comprised 52% of all confirmed lung cancers, and their probability of malignancy was between 18% (for nonsolid nodules) and 63% (for part-solid nodules), compared with a 7% malignancy rate among strictly solid SPNs [69]; however, it should be noted that the prevalence of nonsolid and part-solid lesions is much lower than the prevalence of solid lesion types. High-resolution CT imaging will play an important role in the further investigation of these lesion types because many of the most subtle occurrences of these lesion types are not detectable when thick-slice CT scanning is used because of partial volume effects.

Computer-automated detection of pulmonary nodules

The evaluation of today's high-resolution MSCT data presents a significant challenge to radiologists because they must review up to 500 CT images for a single examination and discriminate normal lung anatomy from small lesions that potentially represent the early onset of lung cancer. The promise of CT for high-resolution imaging of early lung cancer coupled with the challenges in reviewing these large data sets has led to an increased focus on computer-aided detection (CAD) of lung lesions [70–74]. In Fig. 8, two nodules identified using an automated detection algorithm are shown. The nodule identified by the left arrow is a solid type; the nodule identified by the right arrow is a nonsolid type. Both nodules present a challenge for automated detection algorithms—the solid nodule because it has structures connecting it to the chest wall; the nonsolid nodule because it has a lower reconstructed attenuation value when compared with solid nodules. It is initially expected that lung cancer CAD techniques will improve radiologic diagnosis by highlighting suspicious regions that the radiologist might otherwise have overlooked. A recent multireader, multi-institution study for lung cancer detection demonstrated an average reduction in the false-negative rate from 10% to 3% when comparing the performance of a radiologist alone to that of a radiologist using a prototype CAD algorithm [75].

As the spatial resolution and amount of data per patient examination continues to increase, CAD technology will become a necessary tool in the radiologist's evaluation of chest CT examinations.

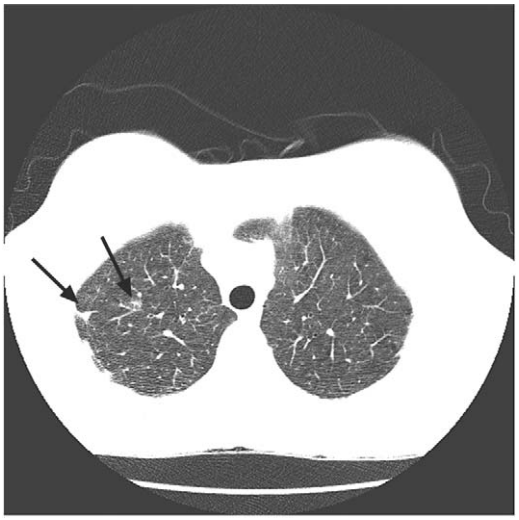

Fig. 8. CAD used to detect lung nodules automatically. In this image a radiologist detected two potential lung cancers in the right lung (*arrows*). One lung nodule is a solid type (*left arrow*); another nodule is a nonsolid type (*right arrow*). Both of these nodules were also detected using a CAD algorithm developed at the GE Global Research Center. The nodule on the *left* is difficult for most CAD algorithms to detect because it has structures attached to the chest wall. The nodule on the *right* is challenging because the reconstructed intensity is lower than most solid lung nodules. The patient was scanned using a GE Lightspeed system at 120 kVp, 60 mA, and 2.5 mm slice thickness. (Courtesy of The Early Lung Cancer Action Program, New York Presbyterian Hospital, Weill Cornell Medical Center, New York, NY.)

CT for noninvasive diagnosis, staging, and treatment planning

Because of the reduced scanning time for a CT examination using advanced MSCT, there has been a renewed interest in the use of contrast-enhanced CT imaging for the diagnosis and staging of lung nodules [76–78]. The use of iodine contrast agent uptake as a measure of malignancy is predicated on the fact that there are distinct differences in the vascular characteristics of benign and malignant nodules. Although positron emission tomography (PET) is more accurate than CT imaging for the detection of mediastinal metastases [79], the role of CT imaging is still recommended as a diagnostic tool because it is valuable for further workup, including biopsy or surgery planning [80]. Furthermore, the role of CT and PET image fusion has shown considerable promise as an optimal method for noninvasive diagnosis and staging of lung cancer [81,82]. CT imaging also plays a primary role in radiation treatment planning [53].

Chronic obstructive pulmonary disease

Chronic obstructive pulmonary disease (COPD) affects roughly 16 million adults in the United States and is the fourth leading cause of chronic morbidity and mortality in the United States [83]. High-resolution CT imaging has been useful in the evaluation of the presence and extent of emphysema and as a tool to quantify morphologic changes caused by chronic bronchitis [84]. Many of these recent advances have been spurred by the technological improvements in MSCT, namely the ability to acquire a large volume of contiguous high-resolution, thin-slice data in less than 10 seconds.

The superiority of CT imaging over chest radiography in the detection and evaluation of the prevalence of bullae in the lung and the diagnosis of emphysema has been well documented [84,85]. Researchers have commented on qualitative methods of assessing the severity of emphysema with CT imaging, correlating radiologic indications with lung function [86–88]. Recent research in the radiologic assessment of emphysema has focused on the development of computational tools that can objectively evaluate the extent of emphysema through the measurement of lung density [89,90]. Because lung density measurements can be affected by scanner calibration, reconstruction parameters [91,92], patient size, and depth of inspiration, the key to reducing inter- and intravariability of these examinations is to model and correct for these effects.

The ability to use CT imaging to detect bronchial wall thickening caused by chronic bronchitis (which is associated with reduced lung function in the case of COPD and asthma) has been well documented in the recent literature [84,93]. The ability to measure small changes in the airway lumen area and in the airway wall area is at the limit of the resolving power of state-of-the-art CT scanners. Because of the scanner's inherent resolution capabilities, quantitative measurement accuracy is limited by the partial volume effect [94]. Several reports have shown that computational methods are more accurate than manual methods [93,95,96], and methods that correct for the scanner point spread function, or resolving power of the CT system, have a higher rate of repeatability [97].

The availability of thinner slices on state-of-the-art scanners (eg, 0.625 mm) and high-resolution scanning protocols could further improve the accuracy of airway measurements. As resolution in CT scanners continues to improve, the ability to measure airways less than 1 mm accurately will become possible, and the sensitivity of the detection of morphologic changes will increase. For example, a high-resolution CT image of an excised pig lung reconstructed from data acquired with a prototype high-resolution volumetric CT research system is shown in Fig. 9. The lumen of an airway that is approximately 0.5 mm in diameter is clearly visible.

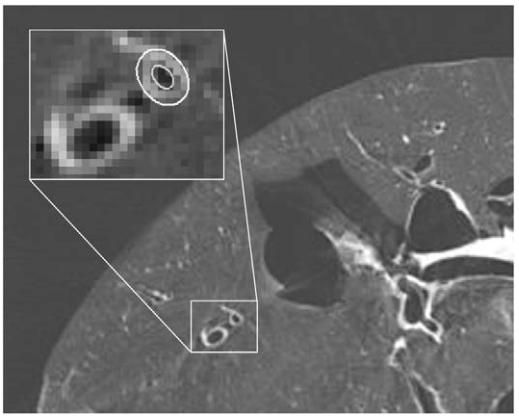

Fig. 9. High-resolution volumetric CT for improved airway wall measurements. A high-resolution volumetric CT research scanner (GE Global Research Center, Niskayuna, NY) capable of 250 μm isotropic resolution was used to image an excised pig lung. The airway lumen (*insert*) was measured with minimal user interaction using prototype software (GE Global Research Center, Niskayuna, NY) and was measured to be about 0.5 mm in diameter.

Pulmonary embolism

It is estimated that the incidence of pulmonary embolism (PE) in the United States is roughly 630,000 cases per year [98]. Since its introduction, [99] CT imaging has been shown to be highly sensitive and specific in the diagnosis of PE when compared with angiography, which is the current standard [100,101]. Recent technological advances in resolution (thinner slices) and speed (faster scans) of multislice CT scanners have improved the detection of PE [102].

CT offers several advantages over other imaging techniques for PE detection. The primary advantage of CT imaging is that scanning can be performed quickly in critically ill patients. Clinicians also have the ability to evaluate patients using CT for other lung-related conditions that could indicate an increased risk of PE such as cardiac disease, chest trauma, pneumonia, and lung cancer.

One impediment to detecting PE in CT images is that the current resolution capability limits the detection of subsegmental PEs [103], although the clinical importance of such cases is a subject of debate. As

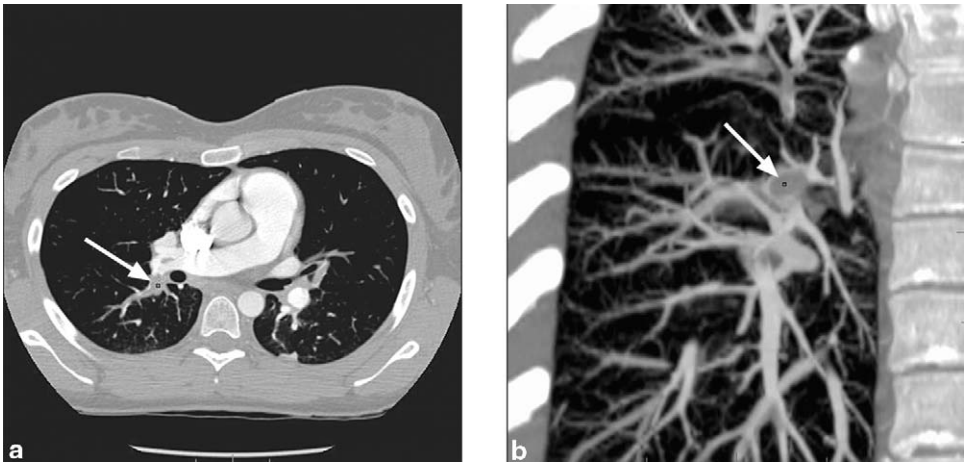

Fig. 10. Multislice CT for the detection of PE. (*a*) On the *left*, an axial CT image shows an occurrence of PE (*arrow*). (*b*) Maximum-intensity projection image of the volume is shown on the *right* in sagittal reformat. The PE (*arrow*) is readily detectable. The patient was imaged using a GE Lightspeed 16. (Courtesy of Lawrence Goodman, MD, Froedtert Hospital, Milwaukee, WI.)

resolution continues to improve and advanced MSCT technology becomes more available, these limitations could possibly be surmounted, as suggested by some researchers [102,104]. Some misdiagnoses are caused by the difficulty in quickly finding an abnormality in a complicated vessel structure [105]. To review the entire chest in high resolution, the radiologist must review between 100 and 300 axial images. This task might be facilitated with advanced segmentation techniques. For example, an occurrence of a PE is shown in an axial image (Fig. 10a), but in a maximum-intensity projection image of a sagittal cross-section (Fig. 10b), the PE is readily detectable and there are considerably less images to review. Some researchers have suggested using CAD methods to detect PE in CT images rapidly [106,107].

Interventional procedures

CT imaging has been a standard in surgery planning, radiation therapy planning, virtual endoscopy, and guidance for percutaneous needle biopsy. Image-guided surgery, a procedure in which the physician uses a two- or three-dimensional image along with the registration of the surgical instruments in the reconstructed volume to guide the procedure, is at the forefront of medical technology. Two-dimensional imaging techniques are limited because the surgeon must virtually conceptualize the three-dimensional and correlate the image with the anatomy. The use of preoperative CT images and three-dimensional visualization offers a more natural view of the anatomy, creating new possibilities for more minimally invasive techniques. Procedures for use in the sinus, spine, and head are becoming more widespread [108–110].

Of particular interest in surgical treatment for oncology is the use of percutaneous, image-guided, in situ tumor ablation techniques [111]. The most advanced of these techniques uses a radiofrequency (RF) thermal source positioned by way of an electrode placed with image guidance into the tumor to be ablated. Although the standard of care for a detected lung cancer is resection, some researchers have proposed RF ablation for pulmonary nodules in patients who are not candidates for surgery [112–114].

One barrier to extending these techniques to other areas in the thorax is the fact that the chest undergoes significant movement during the breathing cycle, which makes it difficult to register the current location of the electrode with a preoperative scan or requires surgical procedures to be performed in the vicinity of the CT scanner. The development of deformable models [115,116], which can predict the organ movement, advanced visualization techniques [117], and multimodality data integration, will extend these techniques in the future.

Summary

X-ray CT technology has been available for more than 30 years, yet continued technological advances have kept CT imaging at the forefront of medical

imaging innovation. Consequently, the number of clinical CT applications has increased steadily. Other imaging modalities might be superior to CT imaging for some specific applications, but no other single modality is more often used in chest imaging today. Future technological developments in the area of high-resolution detectors, high-capacity x-ray tubes, advanced reconstruction algorithms, and improved visualization techniques will continue to expand the imaging capability. Future CT imaging technology will combine improved imaging capability with advanced and specific computer-assisted tools, which will expand the usefulness of CT imaging in many areas.

Acknowledgments

The authors thank Rick Avila, Bob Senzig, Samit Basu, and Rajiv Gupta for their useful comments and insights.

References

[1] Hounsfield G. Computerized transverse axial scanning (tomography): part 1. Description of system. Br J Radiol 1973;46:1016–22.
[2] Cormack A. Representation of a function by its line integrals, with some radiological applications. J Appl Phys 1963;34(9):2722–7.
[3] Mori I. 1986. US Patent No. 4630202.
[4] Nishimura H. 1988. US Patent No. 4789929.
[5] Kalender WA, Seissler W, Klotz E, Vock P. Spiral volumetric CT with single-breath-hold technique, continuous transport, and continuous scanner rotation. Radiology 1990;176(1):181–3.
[6] Crawford CR, King KF. Computed tomography scanning with simultaneous patient translation. Med Phys 1990;17(6):967–82.
[7] Boyd D, Lipton M. Cardiac computed tomography. Proc IEEE 1983;71:298–307.
[8] McCollough CH. Optimization of multi-detector array CT acquisition parameters for CT colonography. Abdom Imaging 2002;27(3):253–9.
[9] Honda JT, Yamamoto S, Tomiyama N, Koyama M, Kozuka T, Mihara N, et al. Evaluation of image quality and spatial resolution of low-dose high-pitch multidetector-row helical high-resolution CT in 11 autopsy lungs and a wire phantom. Radiat Med 2001;19(6):279–84.
[10] Medical Systems GE. Available at: http://www.gemedicalsystems.com/rad/ct/products/light_series/ls16. Accessed January 6, 2004.
[11] Siemens. Available at: http://www.siemens.com. Accessed January 6, 2004.
[12] Toshiba Medical Systems. Available at: http://medical.toshiba.com/clinical/cardiology/aquilionmulti16.htm. Accessed January 6, 2004.
[13] Philips Medical Systems. Available at: http://www.medical.philips.com. Accessed January 6, 2004.
[14] Ross WR, Basu S, Edic PM, Johnson M, Pfoh A, Rao R, et al. Design and image quality results from volumetric CT with a flat-panel imager. In: Antonuk LE, Yaffe MJ, editors. Proceedings of SPIE Medical Imaging. San Diego: SPIE International Society for Optical Engineering; 2001. p. 783–91.
[15] Hu H. Multi-slice helical scan and reconstruction. Med Phys 1999;26(1):5–18.
[16] Kalender WA, Fuchs T. Principles and performance of single- and multislice spiral CT. In: RSNA categorical course in diagnostic radiology physics: CT and US cross-sectional imaging. 2000. p. 127–42.
[17] Feldkamp LA, Davis LC, Kress JW. Practical cone beam algorithm. J Opt Soc Am 1984;A(1):612–9.
[18] Hu H. A new cone beam reconstruction algorithm for the circle-and-line orbit. In: Nuclear Science Symposium and Medical Imaging Conference, Volume 3. IEEE; 1994. p. 1261–5.
[19] Tuy HK. An inversion formula for cone-beam reconstruction. SIAM J Appl Math 1983;43:546–52.
[20] Grangeat P. Analyse d'un systeme d'imagerie 3D par reconstruction a partir de radiographies X en geometrie conique. PhD thesis, Ecole Nationale Superieure des Telecommunications, France, 1987. [in French].
[21] Schaller S, Noo F, Sauer F, Tam K, Lauritsch G, Flohr T. Exact radon rebinning algorithm for the long object problem in helical cone-beam CT. IEEE Trans Med Imaging 2000;19(5):361–75.
[22] Defrise MC. A cone-beam reconstruction algorithm using shift-variant filtering and cone-beam backprojection. IEEE Trans Med Imaging 1994;13(1):186–95.
[23] Katsevitch A. Analysis of an exact inversion algorithm for spiral cone-beam CT. Phys Med Biol 2002;47:2583–97.
[24] Kachelriess M, Schaller S, Kalender WA. Advanced single-slice rebinning in cone-beam spiral CT. Med Phys 2000;27(4):754–72.
[25] Turbell H, Danielsson P. Helical cone-beam tomography. Int J Img Sys Tech 2000;11:91–100.
[26] Medical Systems GE. GE Medical Systems Cardiology EBT series. Available at: http://www.gemedicalsystems.com/cardiology/ebt/index.html. Accessed January 6, 2004.
[27] Sablayrolles JL, Besse F, Giat P. Technical developments in cardiac CT: 2000 update. Rays 2001;26(1):3–13.
[28] Kachelriess M, Ulzheimer S, Kalender WA. ECG-correlated image reconstruction from subsecond multislice spiral CT scans of the heart. Med Phys 2000;27:1881–902.
[29] Pan T, Shen Y. Multi-sector reconstruction for multislice cardiac (CT). Radiology 2000;217:161.
[30] Achenbach S, Giesler T, Ropers D. Detection of coronary artery stenoses by contrast-enhanced, retro-

spectively electrocardiographically gated, multislice spiral computed tomography. Circulation 2001;103: 2535–8.
[31] Cesmeli E, Edic PM, Iatrou M, Pfoh A. A novel reconstruction algorithm for multiphasic cardiac imaging using multislice CT. In: Antonuk LE, Yaffe MJ, editors. Proceedings of the SPIE International Symposium on Medical Imaging. San Diego: SPIE, International Society for Optical Engineering; 2001. p. 645–54.
[32] Huda W, Chamberlain C, Rosenbaum A, Garrisi W. Radiation doses to infants and adults undergoing head CT examinations. Med Phys 2001;28(3):393–9.
[33] Morin R, Gerber T, McCollough C. Radiation dose in computed tomography of the heart. Circulation 2003;107:917–22.
[34] McCollough C, Zink F. Performance evaluation of a multi-slice CT system. Med Phys 1999;26(11): 2223–30.
[35] (ICRP) ICoRP. 1990 Recommendations of the International Commission on Radiological Protection. ICRP Publication 60. Oxford (UK): Pergmon Press; 1991.
[36] McCollough CH, Schueler BA. Calculation of effective dose. Med Phys 2000;27(5):828–37.
[37] Toth T, Limkeman MK. 1997. US Patent No. 5625662.
[38] Harpen M. A simple theorem relating noise and patient dose in computed tomography. Med Phys 1999; 26(11):2231–4.
[39] Hu H, Shen Y. Helical CT reconstruction with longitudinal filtration. Med Phys 1998;25(11):2130–8.
[40] Kachelriess M, Watzke O, Kalender W. Generalized multi-dimensional adaptive filtering for conventional and spiral single-slice, multi-slice, and cone-beam CT. Med Phys 2001;28(4):475–89.
[41] Nuyts J, Dupont P, Stroobants S, Maes A, Mortelmans L, Suetens P. Evaluation of maximum-likelihood based attenuation correction in positron emission tomography. In: Nuclear Science Symposium. Toronto: IEEE; 1998. p. 1836–41.
[42] De Man B, Nuyts J, Dupont P, Marchal G, Suetens P. An iterative maximum-likelihood polychromatic algorithm for CT. IEEE Trans Med Imaging 2001; 20(10):999–1008.
[43] Elbakri IA, Fessler JA. Statistical image reconstruction for polyenergetic x-ray computed tomography. IEEE Trans Med Imaging 2002;21(2):89–99.
[44] Sukovic P, Clinthorne NH. Data weighted vs. non-data weighted dual energy reconstructions for x-ray tomography. In: Nuclear Science Symposium. Toronto: IEEE; 1998. p. 1581–3.
[45] De Man B. 2001. Iterative reconstruction for reduction of metal artifacts in computed tomography. PhD thesis, University of Leuven.
[46] Wang G, Frei T, Vannier MW. A fast iterative algorithm for metal artifact reduction in x-ray CT. Acad Radiol 2000;7(8):607–14.
[47] De Man B. Reduction of metal streak artifacts in x-ray computed tomography using a transmission maximum a posteriori algorithm. IEEE Trans Nuc Sci 2000;47(3):977–81.
[48] Lawler LP, Fishman EK. Multi-detector row CT of thoracic disease with emphasis on 3D volume rendering and CT angiography. Radiographics 2001;21(5): 1257–73.
[49] Salvolini L, Bichi Secchi E, Costarelli L, De Nicola M. Clinical applications of 2D and 3D CT imaging of the airways—a review. Eur J Radiol 2000;34(1): 9–25.
[50] American Cancer Society. Cancer facts and figures 2002. Available at: http://www.cancer.org.docroot/STT/stt_0.asp. Accessed January 6, 2004.
[51] Bach PB, Kelley MJ, Tate RC, McCrory DC. Screening for lung cancer: a review of the current literature. Chest 2003;123(90010):72S–82S.
[52] Beckles MA, Spiro SG, Colice GL, Rudd RM. Initial evaluation of the patient with lung cancer: symptoms, signs, laboratory tests, and paraneoplastic syndromes. Chest 2003;123(90010):97S–104S.
[53] Hopper KD, Singapuri K, Finkel A. Body CT and oncologic imaging. Radiology 2000;215:27–40.
[54] Mathur PN, Edell E, Sutedja T, Vergnon J-M. Treatment of early stage non-small cell lung cancer. Chest 2003;123(90010):176S–80S.
[55] Nakata M, Saeki H, Takata I, Segawa Y, Mogami H, Mandai K, et al. Focal ground-glass opacity detected by low-dose helical CT. Chest 2002;121(5):1464–7.
[56] Patz EF. Imaging bronchogenic carcinoma. Chest 2000;117:90S–5S.
[57] Porter JC, Spiro SG. Detection of early lung cancer. Thorax 2000;55(Suppl 1):556–62.
[58] Swensen SJ. Functional CT: lung nodule evaluation. Radiographics 2000;20(4):1178–81.
[59] Tan BB, Flaherty KR, Kazerooni EA, Iannettoni MD. The solitary pulmonary nodule. Chest 2003; 123(90010):89S–96S.
[60] Toloza EM, Harpole L, Detterbeck F, McCrory DC. Invasive staging of non-small cell lung cancer: a review of the current evidence. Chest 2003;123(90010): 157S–66S.
[61] Yankelevitz DF, Reeves AP, Kotis WJ, Zhao B, Henschke CI. Small pulmonary nodules: volumetrically determined growth rates based on CT evaluation. Radiology 2000;217:251–6.
[62] Henschke CI, McCauley DI, Yankelevitz DF, Naidich DP, McGuinness G, Miettinen OS, et al. Early Lung Cancer Action Project: overall design and findings from baseline screening. Lancet 1999;354(9173): 99–105.
[63] Henschke CI, Naidich DP, Yankelevitz DF. Early Lung Cancer Action Project: initial findings on repeat screenings. Cancer 2001;92(1):153–9.
[64] Sone S, Takashima S, Li F, Yang Z, Honda T, Maruyama Y, et al. Mass screening for lung cancer with mobile spiral computed tomography scanner. Lancet 1998;351(9111):1242–5.
[65] Mulshine JL, Smith RA. Lung cancer 2: screening and

early diagnosis of lung cancer. Thorax 2002;57(12): 1071–8.
[66] Yankelevitz DF, Gupta R, Zhao B, Henschke CI. Small pulmonary nodules: evaluation with repeat CT—preliminary experience. Radiology 1999;212(2): 561–6.
[67] Winer-Muram H, Jennings S, Tarver R, Aisen A, Tann M, Conces D, et al. Volumetric growth rate of stage I lung cancer prior to treatment: serial CT scanning. Radiology 2002;223:789–805.
[68] Kin E, Johkoh T, Lee K, Han J, Fujimoto K, Adohara J, et al. Quantification of ground-glass opacity on high-resolution CT of small peripheral adenocarcinoma of the lung: pathologic and prognostic implications. AJR Am J Roentgenol 2001;177(6):1417–22.
[69] Henschke C, Yankelevitz DF, Mirtcheva R, McGuinness G, McCauley DI, Miettinen OS. CT screening for lung cancer: frequency and significance of part-solid and nonsolid nodules. AJR Am J Roentgenol 2002;178(5):1053–7.
[70] Armato III S, Giger M, MacMahon H. Automated detection of lung nodules in CT scans: preliminary results. Med Phys 2001;28(8):1552–61.
[71] Niki N, Kawata Y, Kubo H, Ohmatsu M, Kakinuma R, Kaneko M, et al. A CAD system for lung cancer based on 3D CT images. In: Lemke HU, Vannier MW, Inamura K, Farman AG, Doi K, Reiber JHC, editors. Proceeding of International Congress of Computer Assisted Radiology and Surgery. Paris: Springer; 2002. p. 701–5.
[72] McNitt-Gray M, Hart E, Wyckoff N, Sayre J, Goldin J, Aberle D. A pattern classification approach to characterizing solitary pulmonary nodules imaged on high resolution CT: preliminary results. Med Phys 1999; 26(6):880–8.
[73] Takizawa H, Yamamoto S, Matsumoto T, Tateno Y, Linuma T, Matsumoto M. Recognition of lung nodules from x-ray CT images using 3D MRF models. In: Tezak EJ, Inamura K, Lemke HU, et al, editors. Proceeding of International Congress of Computer Assisted Radiology and Surgery. Berlin: Elsevier Science; 2001. p. 605–14.
[74] Armato III SG, Li F, Giger ML, MacMahon H, Sone S, Doi K. Lung cancer: performance of automated lung nodule detection applied to cancers missed in a CT screening program. Radiology 2002;225(3): 685–92.
[75] McCulloch C, Yankelevitz D, Henschke C, Patel S, Kazerooni E, Sirohey S. Reader variability and computer aided detection of suspicious lesions in low-dose CT lung screening exams. Radiology 2003; 226(2):37A.
[76] Zhang M, Kono M. Solitary pulmonary nodules: evaluation of blood flow patterns with dynamic CT. Radiology 1997;205(2):471–8.
[77] Miles KA, Griffiths MR, Fuentes MA. Standardized perfusion value: universal CT contrast enhancement scale that correlates with FDG PET in lung nodules. Radiology 2001;220(2):548–53.
[78] Swensen SJ, Viggiano RW, Midthun DE, Muller NL, Sherrick A, Yamashita K, et al. Lung nodule enhancement at CT. Multicenter study. Radiology 2000; 214(1):73–80.
[79] Toloza EM, Harpole L, McCrory DC. Noninvasive staging of non-small cell lung cancer: a review of the current evidence. Chest 2003;123(90010): 137S–46S.
[80] Silvestri GA, Tanoue LT, Margolis ML, Barker J, Detterbeck F. The noninvasive staging of non-small cell lung cancer: the guidelines. Chest 2003;123(90010): 147S–56S.
[81] Vansteenkiste JF, Stroobants SG, Dupont P, De Leyn PR, De Wever WF, Verbeken EK, et al. FDG-PET scan in potentially operable non-small cell lung cancer: do anatometabolic PET-CT fusion images improve the localisation of regional lymph node metastases? Eur J Nucl Med 1998;25(11):1495–501.
[82] Magnani P, Carretta A, Rizzo G, Fazio F, Vanzulli A, Lucignani G, et al. FDG/PET and spiral CT image fusion for mediastinal lymph node assessment of non-small cell lung cancer patients. J Cardiovasc Surg [Torino] 1999;40(5):741–8.
[83] National Heart, Lung, and Blood Institute, National Institutes of Health. Data fact sheet: chronic obstructive pulmonary disease (COPD). Available at: http://www.nhlbi.nih.gov/health/public/lung/other/copd_fact.htm. Accessed January 6, 2004.
[84] Muller NL, Coxson H. Chronic obstructive pulmonary disease 4: imaging the lungs in patients with chronic obstructive pulmonary disease. Thorax 2002;57(11): 982–5.
[85] Thurlbeck WM, Muller NL. Emphysema: definition, imaging, and quantification. AJR Am J Roentgenol 1994;163:1017–25.
[86] Nakano Y, Muro S, Sakai H, Hirai T, Chin K, Tsukino M, et al. Computed tomographic measurements of airway dimensions and emphysema in smokers. Correlation with lung function. Am J Respir Crit Care Med 2000;162(3):1102–8.
[87] Miller RR, Muller NI, Vedal S, Morrison NJ, Staples CA. Limitations of computed tomography in the assessment of emphysema. Am Rev Respir Dis 1989; 139:980–3.
[88] Kuwano K, Matsuba K, Ikeda T, Murakami J, Araki A, Nishitani H, et al. The diagnosis of mild emphysema: correlation of computed tomography and pathology scores. Am Rev Respir Dis 1990;141: 169–78.
[89] Muller N, Staples C, Miller R, Abboud R. Density mask. An objective method to quantitate emphysema using computed tomography. Chest 1988;94(4): 782–7.
[90] Brown MS, McNitt-Gray MF, Goldin JG, Greaser LE, Hayward UM, Sayre JW, et al. Automated measurement of single and total lung volume from CT. J Comp Ass Tomo 1999;23:632–40.
[91] Gierada DS, Yusen RD, Pilgram TK, Crouch L, Slone RM, Bae KT, et al. Repeatability of quantitative CT

indexes of emphysema in patients evaluated for lung volume reduction surgery. Radiology 2001;220(2): 448–54.
[92] Bankier AA, De Maertelaer V, Keyzer C, Gevenois PA. Pulmonary emphysema: subjective visual grading versus objective quantification with macroscopic morphometry and thin-section CT densitometry. Radiology 1999;211(3):851–8.
[93] Nakano Y, Muller NL, King GG, Niimi A, Kalloger SE, Mishima M, et al. Quantitative assessment of airway remodeling using high-resolution CT. Chest 2002;122(90060):271S–5S.
[94] King GG, Muller NL, Pare PD. Evaluation of airways in obstructive pulmonary disease using high-resolution computed tomography. Am J Respir Crit Care Med 1999;159(3):992–1004.
[95] Wood SA, Zerhouni EA, Hoford JD, Hoffman EA, Mitzner W. Measurement of three-dimensional lung tree structures by using computed tomography. J Appl Physiol 1995;79(5):1687–97.
[96] McNamara AE, Muller NL, Okazawa M, Arntorp J, Wiggs BR, Pare PD. Airway narrowing in excised canine lungs measured by high-resolution computed tomography. J Appl Physiol 1992;73(1):307–16.
[97] Reinhardt JM, D'Souza ND, Hoffman D. Accurate measurement of intrathoracic airways. IEEE Trans Med Imaging 1997;16(6):820–7.
[98] Dalen J. Pulmonary embolism: what have we learned since Virchow?: natural history, pathophysiology, and diagnosis. Chest 2002;122:1440–56.
[99] Sinner WN. Computed tomographic patterns of pulmonary thromboembolism and infraction. J Comp Ass Tomo 1978;2:395–9.
[100] Rathbun SW, Raskob GE, Whitsett TL. Sensitivity and specificity of helical computed tomography in the diagnosis of pulmonary embolism: a systematic review. Ann Intern Med 2000;132:227–32.
[101] Mullins MD, Becker DM, Hagspiel KD, Philbrick JT. The role of spiral volumetric computed tomography in the diagnosis of pulmonary emboli. Arch Intern Med 2000;160(3):293–8.
[102] Ghaye B, Szapiro D, Mastora I, Delannoy V, Duhamel A, Remy J, et al. Peripheral pulmonary arteries: how far in the lung does multi-detector row spiral CT allow analysis? Radiology 2001;219(3):629–36.
[103] Goodman LR, Curtin JJ, Mewissen MW, Foley WD, Lipchik RJ, Crain MR, et al. Detection of pulmonary embolism in patients with unresolved clinical and scintigraphic diagnosis: helical CT vs. angiography. AJR Am J Roentgenol 1995;164:1369–74.
[104] Schoepf UJ, Holzknecht N, Helmberger TK, Crispin A, Hong C, Becker CR, et al. Subsegmental pulmonary emboli: Improved detection with thin-collimation multi-detector row spiral CT. Radiology 2002; 222(2):483–90.
[105] Bates SM, Ginsberg JS. Helical computed tomography and the diagnosis of pulmonary embolism. Ann Intern Med 2000;132:240–1.
[106] Remy-Jardin M, Remy J, Cauvain O, Petyt L, Wanebroucq J, Beregi JP. Diagnosis of central pulmonary embolism with helical CT: role of two-dimensional multiplanar reformations. AJR Am J Roentgenol 1995;165(5):1131–8.
[107] Schoepf UJ, Das M, Schneider A, Anderson M, Wood S, Costello P. Computer aided detection (CAD) of segmental and subsegmental pulmonary emboli on 1-mm multidetector-row CT (MDCT) studies. Paper 579 in Session G02. Chicago: Radiological Society of North America; 2002.
[108] Peters TM. Image-guided surgery: from x-rays to virtual reality. Comput Methods Biomech Biomed Engin 2000;4(1):27–57.
[109] Hassfeld S, Muhling J. Computer assisted oral and maxillofacial surgery—a review and an assessment of technology. Int J Oral Maxillofac Surg 2001;1: 2–13.
[110] Sama AA, Khan SN, Girardi FP, Cammisa Jr CF. Computerized frameless stereotactic image guidance in spinal surgery. Orthop Clin N Am 2002;2:375–80.
[111] Gazelle GS, Goldberg SN, Solbiati L, Livraghi T. Tumor ablation with radio-frequency energy. Radiology 2000;217(3):633–46.
[112] Dupuy DE, Mayo-Smith WW, Abbott GF, DiPetrillo T. Clinical applications of radio-frequency tumor ablation in the thorax. Radiographics 2002;22(90001): 259S–69S.
[113] Zagoria RJ, Chen MY, Kavanagh PV, Torti FM. Radio frequency ablation of lung metastases from renal cell carcinoma. J Urol 2001;166(5):1827–8.
[114] Goldberg SN, Gazell GS. Radio-frequency in the rabbit lung: efficacy and complications: in vivo study in rabbit lung. Acad Radiol 1995;2:776–84.
[115] Suzuki S, Suzuki N, Hattori A, Takatsu A, Uchiyama A. Deformable organ model using the sphere-filled method for virtual surgery. In: Enderle JD, editor. Proceedings of the 22nd Annual International Conference of the IEEE. Toronto: IEEE; 2000. p. 2416–8.
[116] Tseng D-C, Lin J-U. A hybrid physical deformation modeling for laparoscopic surgery simulation. In: Enderle JD, editor. Engineering in Medicine and Biology Society. Proceedings of the 22nd Annual International Conference of the IEEE. Toronto: IEEE; 2000. p. 3032–4.
[117] Satava RM, Jones SB. Current and future applications of virtual reality for medicine. Proc IEEE 1998;86(3): 484–9.